

Supplementary Materials and Methods

Cell viability assay

Cells were seeded onto a 96-well plate and cultured for 72 h. Then 5 $\mu\text{g}/\text{mL}$ of 3-(4,5-dimethylthiazol-2-yl)-5-(3-carboxymethoxyphenyl)-2-(4-sulfophenyl)-2H-tetrazolium (MTS reagent, Promega, WI, USA) were added into each well and incubated at 37 $^{\circ}\text{C}$ for 90 min. The absorbance was measured on a Biotek EL \times 800 spectrophotometer at 490 nm.

Cellular ATP measurement

Intracellular ATP content was measured using a Luminescence ATP Detection Assay Kit (Perkin Elmer, MA, USA). Cells (8×10^3 cells/well) were seeded onto a 96-well plate and cultured for 24 h. Then 50 μL of mammalian cell lysis solution (provided in the kit) were added to each well and the plate was shaken at 700 rpm for 5 min. Then 50 μL of ATPLite substrate solution (provided in the kit) were added and the plate was shaken for another 5 min. The plate was placed in the dark for 10 min and luminescence was measured using an EnSpireTM 2300 Multilabel reader (Perkin Elmer).

RNA extraction and quantitative RT-PCR

RNAs were extracted using the TRIzol reagent (Ambion, MA, USA). RNA was reverse-transcribed using the RevertAid First-Strand cDNA Synthesis kit (Thermo Scientific, MA, USA). Real-time q-PCR analysis was performed with a 7500 Real Time PCR System (Applied Biosystems, MA, USA) using the PowerUpTM SYBR Green Real-Time PCR kit (Applied Biosystems). *β -Actin* was used as an internal control for normalization. The relative fold changes in

gene expression were calculated using the $2^{-\Delta\Delta C_t}$ method. Primer sequence are shown in Table S6.

Measurement of mitochondrial membrane potential

The cellular mitochondrial membrane potential was determined by using the JC-1 (5,5',6,6'-tetrachloro-1,1',3,3'-tetraethylbenzimidazolylcarbocyanine) probe (Life Technologies, MA, USA). Cells (3×10^5) were harvested and suspended in 1 × phosphate buffered saline (PBS). Cells were incubated with 10 $\mu\text{g/ml}$ JC-1 for 10 min at 37 °C. Then the fluorescence was analyzed by BD FACSCanto™ II flow cytometry (BD Biosciences, NJ, USA). JC-1 activity is indicated by a fluorescence emission shift from green (monomer) to red (J-aggregate). The JC-1 monomer and J-aggregate could be excited and detected separately in the 488 nm and 561 nm channels, respectively. The ratio of the intensity of the J-aggregate to the monomer represents the mitochondrial membrane potential levels.

Cellular neutral lipid content analysis

Neutral lipid content was analyzed by using LipidTOX™ Red staining (Life Technologies). The LipidTOX™ Red probe is diluted 1:3000 in 1 × PBS to make a staining buffer. Then 3×10^5 cells were harvested and incubated with the staining buffer for 30 min at room temperature. The fluorescence was analyzed by BD FACSCanto™ II flow cytometry (BD Biosciences) in the 561 nm channel.

Apoptosis assay

Cellular apoptosis was determined by using an Annexin V-APC apoptosis detection kit (KeyGEN Biotech, Nanjing, China). Cells (3×10^5) were harvested and incubated with the Annexin

V-APC probe for 10 min at room temperature. The fluorescence was analyzed by BD FACSCanto™ II flow cytometry (BD Biosciences) in the 633 nm channel.

Mitochondrial isolation

Cells (5×10^6) were harvested and centrifuged at 800 rpm for 5 min at 4 °C. The cell pellets were washed with cold 1×PBS and resuspended in 1 ml of MSHE + BSA isolation buffer (210 mM mannitol, 70 mM sucrose, 5.0 mM HEPES, 1.0 mM EGTA, 0.5% (w/v) fatty acid free bovine serum albumin [BSA] and complete protease inhibitor cocktail, pH 7.2). After chilling on ice for 3 min, the cells were disrupted by 40 strokes of a glass homogenizer. Then the homogenate was vortexed for 15 seconds and chilled on ice for 5 min. The homogenate was centrifuged at 2000 rpm for 10 min at 4 °C to remove unbroken cells and nuclei. The supernatant fraction was collected and centrifuged at 12,000 rpm for 30 min at 4 °C. Then the supernatant fraction was filtered through a 0.1 mm Ultrafree-MC filter (Millipore) to obtain the cytosolic fraction. The pellet was resuspended in 200 µL MSHE + BSA buffer and re-centrifuged at 13,000 rpm for 10 min at 4 °C to obtain the mitochondrial fraction.

Oxygen consumption assay

The MitoXpress®Xtra oxygen consumption assay kit (Luxel Bioscience, Cork, Ireland) was used for the measurement of extracellular oxygen consumption. Cells were seeded onto a 96-well plate and cultured overnight. The contents of the MitoXpress® Xtra vial were reconstituted in 1 ml of culture media before use. Pre-warmed culture medium (150µL) and 10 µL of reconstituted MitoXpress® Xtra reagent were added to each well. Two wells free from the addition of

MitoXpress® Xtra reagent were used as the blank control. Then two drops of pre-warmed HS Mineral Oil were added onto the surface. The plate was immediately read in the EnVision® Multi-mode Plate Reader (Perkin Elmer). The plate was measured kinetically for at least 90 min and the excitation wavelength was 380 nm and emission wavelength was 650 nm. Time-resolved fluorescence measurement was used to reduce non-specific background and increase probe sensitivity. The delay time was 30 μ s and gate time was 100 μ s. MitoXpress® Xtra intensity versus time was plotted and the slope values for each sample represented the oxygen consumption rate.

UPLC-MS/MS analysis

The UPLC-MS/MS analysis was performed on an Agilent 1290 UHPLC system coupled to an Agilent 6460 Triple Quadrupole MS System (Agilent Technologies, Santa Clara, CA, USA). The samples were separated using a Phenomenex Luna Omega Polar C18 column (100 mm \times 2.1 mm, 1.6 μ m) with a linear gradient elution system of mobile-phase (A) 0.1% formic acid (B) methanol. The gradient elution conditions were 0 - 0.5 min, 1% B; 7 min, 100% B; 9 min, 100% B. The column temperature was 30 $^{\circ}$ C. The injection volume was 5 μ L. The flow rate was maintained at 0.3 mL/min. The analytes eluted from the column were ionized in an Agilent Jet Stream Electrospray Ionization (AJS ESI) source in positive mode (ESI+).

Lauroylcarnitine (C12), myristoylcarnitine (C14), palmitoylcarnitine (C16) were purchased from Cambridge Isotope Laboratories, Inc. (CIL, MA, USA). The parameters of ion source were as follows: gas temperature 300 $^{\circ}$ C; gas flow rate, 10 L/min; nebulizer, 45 psi, SheathGasHeater, 300 $^{\circ}$ C; SheathGasFlow, 12; and capillary voltage, 4000 V. The chromatographic retention time was 7.04, 7.36, and 7.60 min for C12, C14, and C16 carnitine, respectively. The multiple reaction monitoring

(MRM) was used to acquire data in optimized MRM transition (precursor > product). The precursors (m/z) of 344.2, 372.3, and 400.3 were set for the M0 of lauroylcarnitine (C12), myristoylcarnitine (C14), palmitoylcarnitine (C16), respectively. The M0, M1, ..., Mn were analyzed for isotope labeled acylcarnitines, where n is the chain length of fatty acyls of acylcarnitine. The product 85 (m/z) was selected for all MRM transitions. The values of fragmentor were 152 V, 162 V, and 172 V for C12, C14, and C16 carnitine, respectively. The values of collision energy (CE) were 23, 25, and 29 V for C12, C14, and C16 carnitine, respectively. The dwelling time was set at 5 ms.

Table S1. The official full name and function of *FAO* genes.

Gene	Full name	Function
ACSL4	Acyl-CoA synthetase (long-chain)	Convert free long-chain fatty acids into fatty acyl-CoA esters
ACSL5		
CPT1A	Carnitine palmitoyltransferase	Promote carnitine-dependent transport across the mitochondrial membrane
CPT1B		
CPT1C		
CPT2		
CRAT	Carnitine O-acetyltransferase	Regulate the acyl-CoA/CoA ratio
ACADS	Acyl-CoA dehydrogenase (C-2 to C-3)	Catalyze the initial step of FAO
ACAD9		
ACADM	Acyl-CoA dehydrogenase (C-4 to C-12)	
ACAD10		
ACADL	Acyl-CoA dehydrogenase (long chain)	
ACAD11		
HADHA	Hydroxyacyl-CoA dehydrogenase/	Catalyze the last three steps of FAO
HADHB	3-ketoacyl-CoA thiolase/enoyl-CoA hydratase	
ACAA2	Acetyl-CoA acyltransferase 2	Catalyze the last step of FAO
ECI1	Enoyl-CoA delta isomerase	Regulate FAO for

EC12		unsaturated fatty acids
------	--	-------------------------

Table S2. Clinical characteristics and CPT1A expression level in 48 non-keratinizing undifferentiated NPC patients who received radiation therapy.

Clinical Characteristics	CPT1A Low expression	CPT1A High expression	<i>p</i> -value
Age (yr), mean \pm S.D.	47.81 \pm 11.56	46.18 \pm 7.64	0.58 ^a
Gender			
Males (n)	8	18	0.32 ^b
Females (n)	8	4	
Neck lymph node			
Metastasis			
Negative (n)	11	7	0.74 ^b
Positive (n)	10	8	
No information (n)	5	7	
EBER status			
Low	6	3	0.4 ^b
High	20	19	

^aWelch's *t* test.

^bPearson's χ^2 test.

Table S3. LC/MS/MS analysis of CPT1A-interacting proteins.

Protein ID	Description	Protein Score	Unique peptide
tr B2RAQ8 B2RAQ8_HUMAN	CPT1A	1781.32	19
sp P51148 RAB5C_HUMAN	Rab5C	326.15	3
sp P51149 RAB7A_HUMAN	Rab7A	292.17	7
tr X6RFL8 X6RFL8_HUMAN	Rab14	284.03	4
tr B4DGL0 B4DGL0_HUMAN	HSP90AB1	208.99	2
sp P20339 RAB5A_HUMAN	Rab5A	192.8	2
sp P61006 RAB8A_HUMAN	Rab8A	167.78	1
tr Q53T70 Q53T70_HUMAN	Rab10	160	1
tr I7HJJ0 I7HJJ0_HUMAN	SLC25A6	147.67	1
tr F5H157 F5H157_HUMAN	Rab35	136.64	1
sp P61019 RAB2A_HUMAN	Rab2A	121.32	3
sp Q9UNL2 SSRG_HUMAN	SSR3	97.24	1
tr A0A075B6Q0 A0A075B6Q0_HUMAN	RAP1A	95.69	2
tr H3BRU6 H3BRU6_HUMAN	PCBP2	90.21	2
tr F8VV32 F8VV32_HUMAN	LYZ	88.46	1
tr A0A024R599 A0A024R599_HUMAN	SLC3A2	71.82	1
tr A0A0A0MSI0 A0A0A0MSI0_HUMAN	PRDX1	68.94	3
tr E9PB61 E9PB61_HUMAN	ALYREF	46.03	1
tr J3KSN1 J3KSN1_HUMAN	LASP1	44.58	1
sp P31151 S10A7_HUMAN	S100A7	44.55	1

tr A0A023QSC6 A0A023QSC6_HUMAN	ND3	43.87	1
tr K7EK77 K7EK77_HUMAN	ATP5A1	43.67	1
tr F5GXX5 F5GXX5_HUMAN	DAD1	43.53	1
tr C9JNV2 C9JNV2_HUMAN	BUD31	41.72	1
sp P10599 THIO_HUMAN	TXN	41.06	1
tr I6L8B7 I6L8B7_HUMAN	FABP5	38.7	1
tr Q5HY57 Q5HY57_HUMAN	EMD	38.69	1
sp P02647 APOA1_HUMAN	APOA1	36.17	1
tr Q5U0A0 Q5U0A0_HUMAN	PSMA	35.2	1
sp P05109 S10A8_HUMAN	S100A8	34.85	1
tr I1VE16 I1VE16_HUMAN	SEC22B	34.58	1
tr E5RFP6 E5RFP6_HUMAN	VDAC3	34.53	1
sp Q4VX76 SYTL3_HUMAN	SYTL3	34.44	1
tr B4DKN9 B4DKN9_HUMAN	RhoA	33.83	1

Table S4. The residue composition of the predicted Site 1 and Site 2 on CTP1A.

Site	Residues
Site 1	R82, A85, R96, T98, Y99, N100, H101, L102, S103, S104, L106, A109, R110, N111, L112, T113, N114, P115, N116, T117, V118, I119, I120, E137, E138, A139, K140, Q141, F142, A143, E145, N146, G147, L148, L149, A168, , K170, K171, I172, Q174, N175
Site 2	Y6, N7, Y8, K13, D19, M20, G21, V22, G23, K24, S25, C26, L28, H29, T32, E33, P41, T43, I44, G45, V46, E47, F48, G49, T50, R51, I52, K61, L62, Q63, I64, Q65, D66, T67, A68, A75, A76, T77, R78, Y80, K125

Table S5. The predicted top 20 strongest coupled interacting residue pairs between CTP1A and Rab14.

CTP1A	Rab14	DI ^a
HIS25	PRO115	0.72219
HIS37	ASN100	0.71843
GLN30	GLU138	0.69234
ARG29	ASN116	0.68364
ARG22	LYS171	0.67704
LEU36	ASN116	0.67602
ARG22	SER103	0.65806
ARG22	ASN100	0.65218
GLN30	GLY147	0.64417
HIS25	ASN100	0.63565
ARG29	GLU138	0.63004
ARG29	GLU137	0.62769
ARG29	LYS140	0.62019
ARG22	GLU138	0.61819
ILE19	LYS140	0.61778
LYS42	HIS101	0.61073
ILE19	GLU138	0.59175
LEU36	PRO115	0.59029
ARG29	PRO115	0.58182

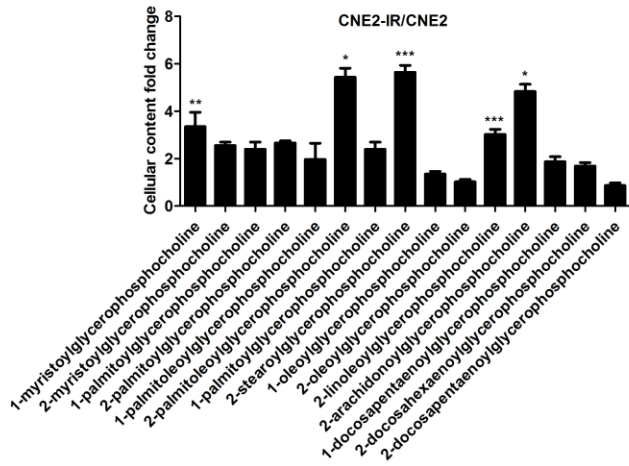
ILE19	GLN141	0.58162
-------	--------	---------

^aDI is the direct coupling value.

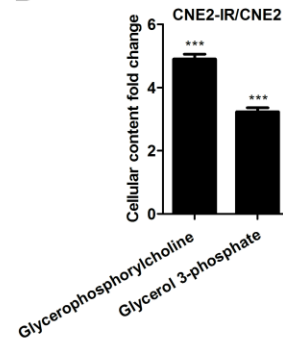
Table S6. The primers used for qRT-PCR

Gene	Forward primer sequence	Reverse primer sequence
<i>ACSL4</i>	ACTGGCCGACCTAAGGGAG	GCCAAAGGCAAGTAGCCAATA
<i>ACSL5</i>	CTCAACCCGTCTTACCTCTTCT	GCAGCAACTTGTTAGGTCATTG
<i>CPT1A</i>	TCCAGTTGGCTTATCGTGGTG	TCCAGAGTCCGATTGATTTTTGC
<i>CPT1B</i>	CCTGCTACATGGCAACTGCTA	AGAGGTGCCCAATGATGGGA
<i>CPT1C</i>	GGGCCGCTTTCTTTGTGTC	AGAAGACGATTAGGGTGAAGGAT
<i>CPT2</i>	CTGGAGCCAGAAGTGTTCCAC	AGGCACAAAGCGTATGAGTCT
<i>CRAT</i>	TTCACCGTGTGCCTAGATGC	CAGCGTCTTGTCGAACCAG
<i>ACADS</i>	AGGGCGACTCATGGGTTCT	GGGATGCGACAGTCCTCAAAG
<i>ACAD9</i>	CTCAAGACTAGGGGAGATCATCA	ACGCCAGTTTAGGCAAGTATTT
<i>ACADM</i>	GGAAGCAGATACCCCAAGGAAT	AGCTCCGTCACCAATTAACAT
<i>ACAD10</i>	CAAACACTCGGCCTGTGAAAA	ACTAGATCACGATTAGCCAGCC
<i>ACADL</i>	TCAGAGCATCGGTTTCAAAGG	AGGGCTCGGTTAGACAGAAAG
<i>ACAD11</i>	TTGGATTCCCCGTTCCCAAG	AAATCACGGAAGATTCGACCC
<i>HADHA</i>	ATATGCCGCAATTTTACAGGGT	ACCTGCAATAAAGCAGCCTGG
<i>HADHB</i>	TACGGGTTTGTTGCATCGGAC	GCCACATTGCTTGTTTTCACTT
<i>ACAA2</i>	AGACAATGCAGGTAGACGAGC	ACCCATGATAGAGGGATCACATC
<i>EC11</i>	CTGCGGTTGTACCAGTCCAA	GATGCGGTAGTCACAGGTCA
<i>EC12</i>	ATGGGACGCATGGAATGCC	TTCAAACCCAGTTGATTTCTGT
<i>Rab14</i>	CAGGAGCGATTTAGGGCTGTT	TGAGATTCTTGCATCTGTCAAC

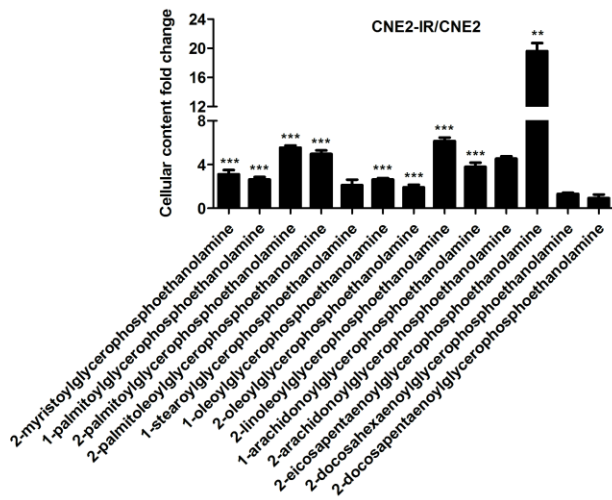
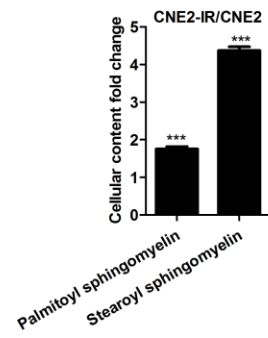
A



B



C



D

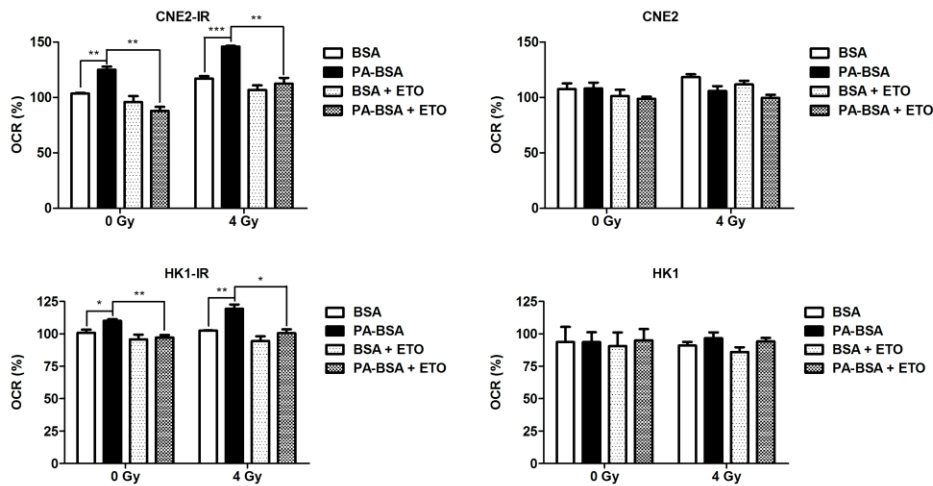
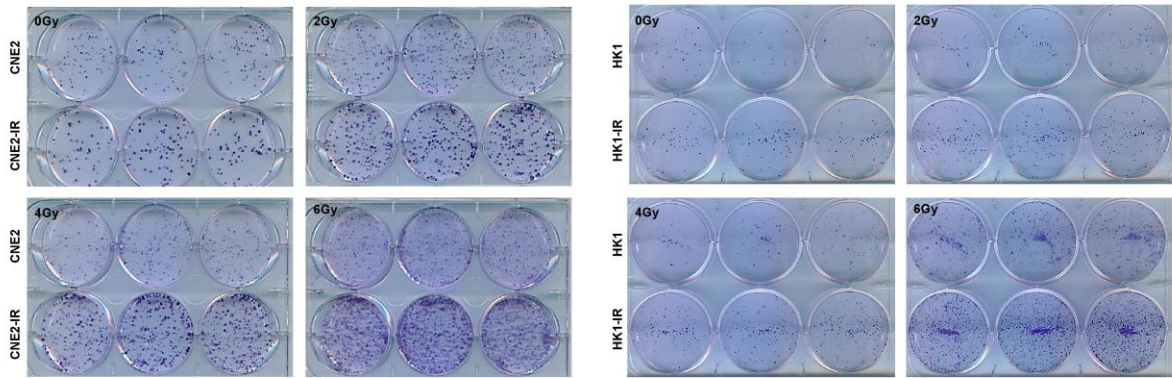
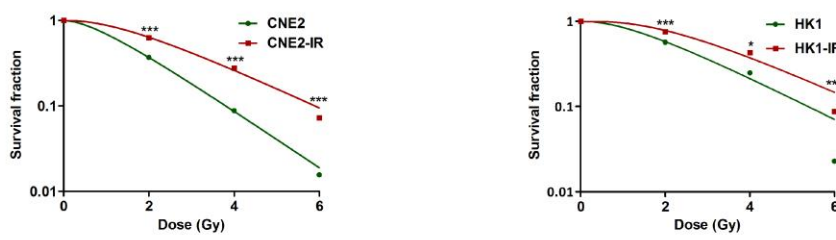


Figure S1

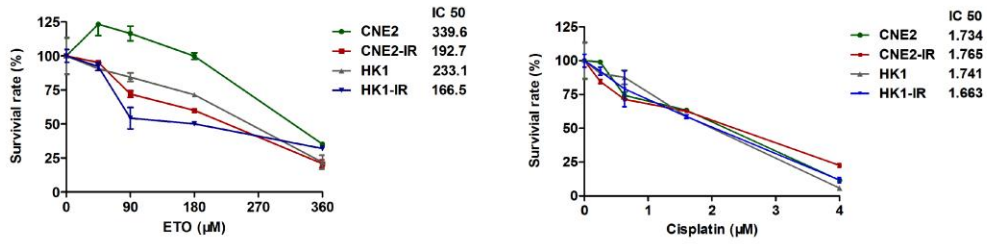
A



B



C



D

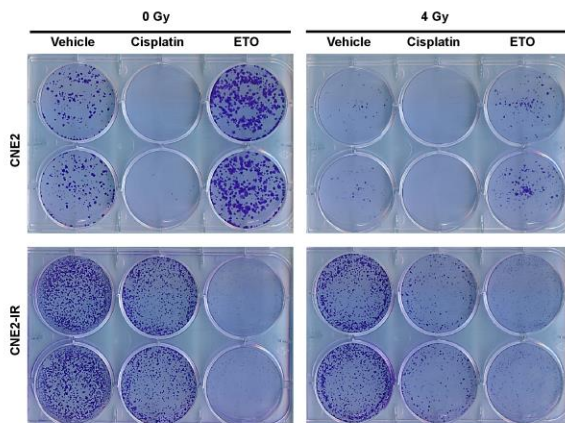


Figure S2

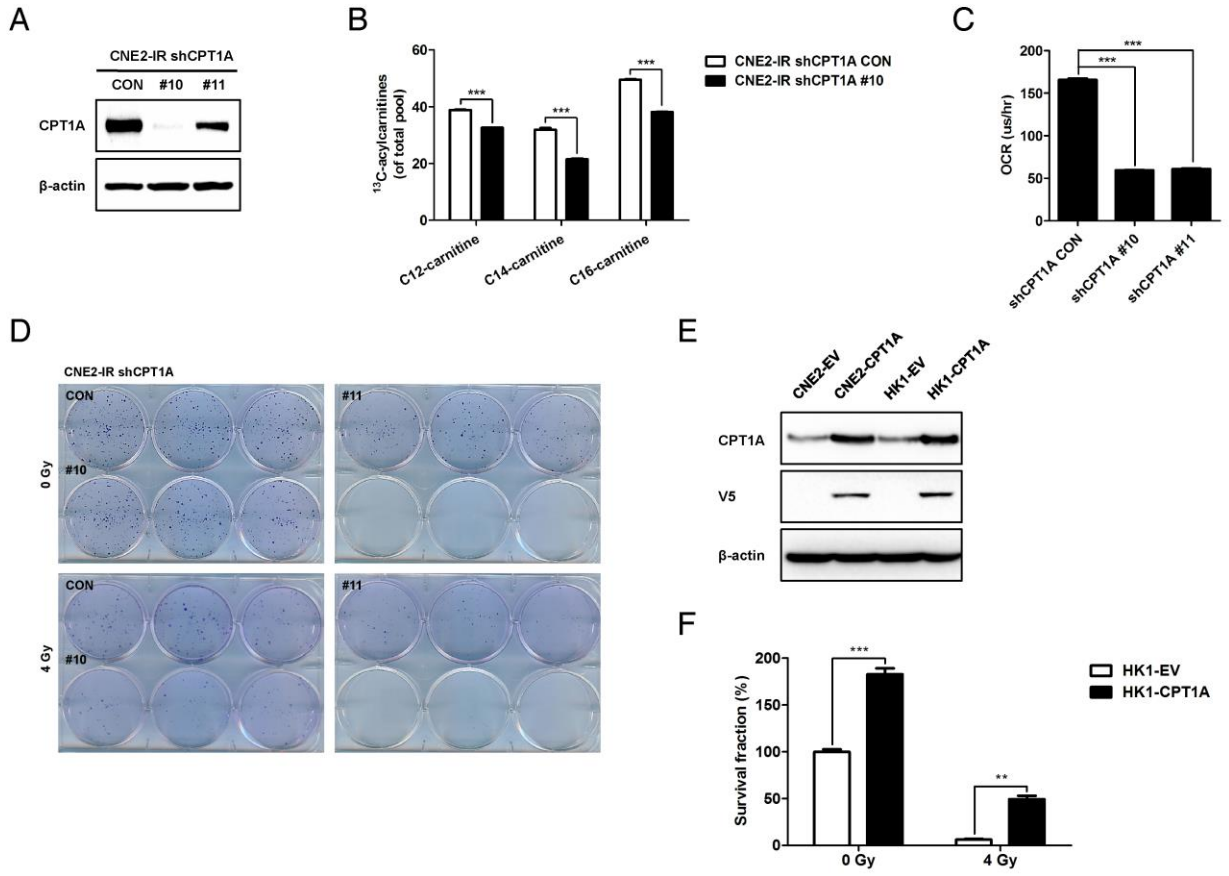


Figure S3

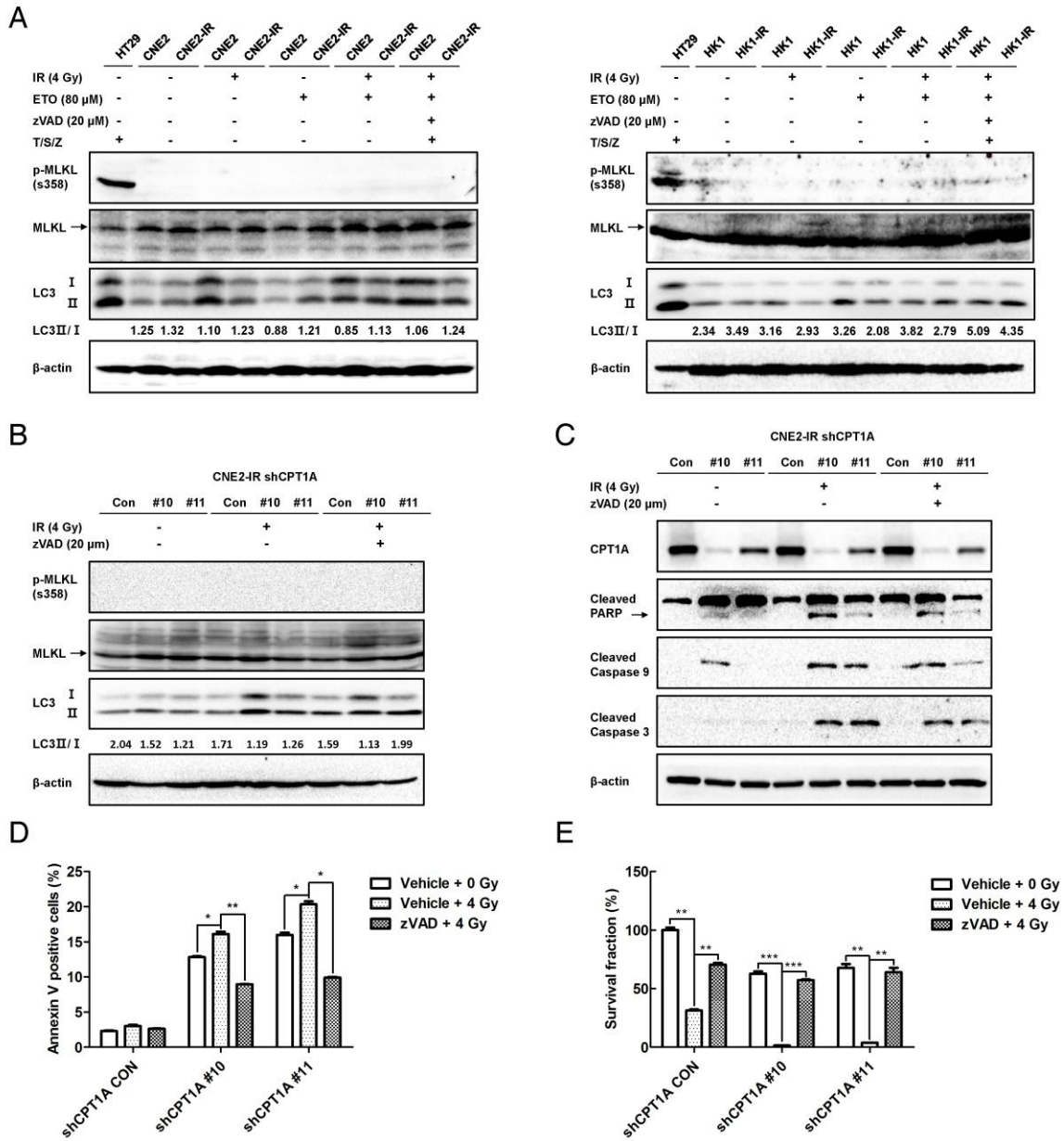


Figure S4

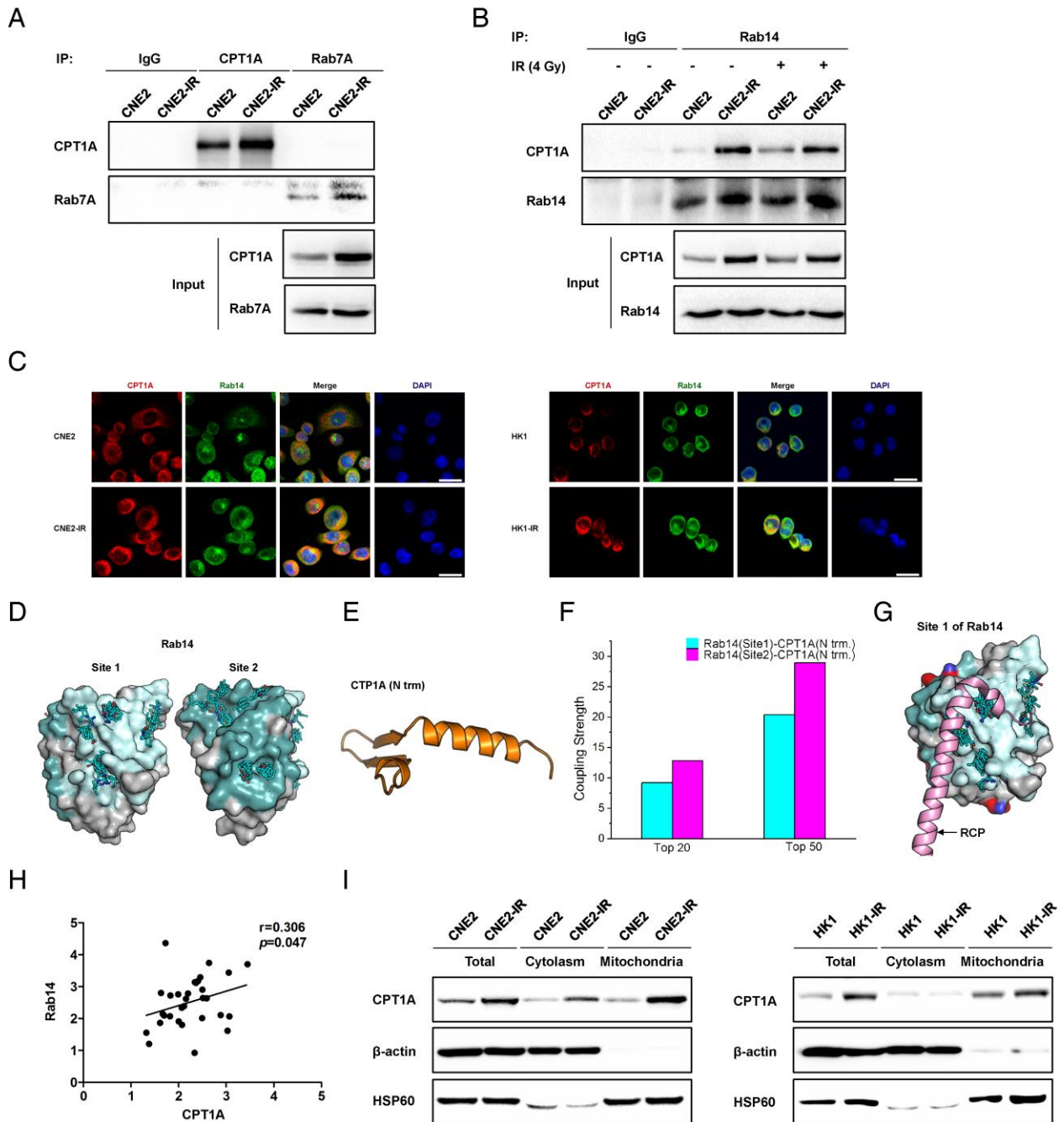


Figure S5

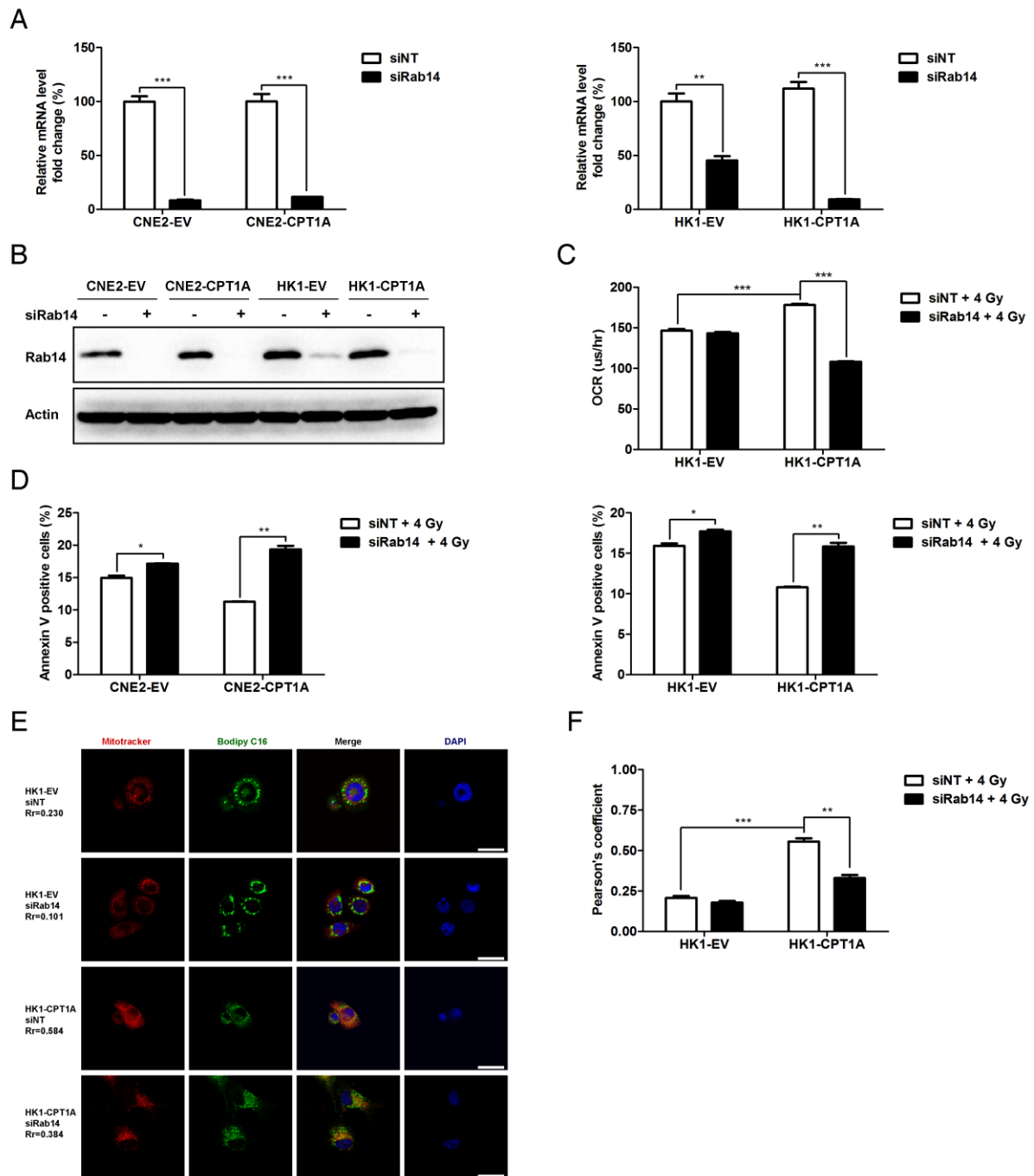


Figure S6

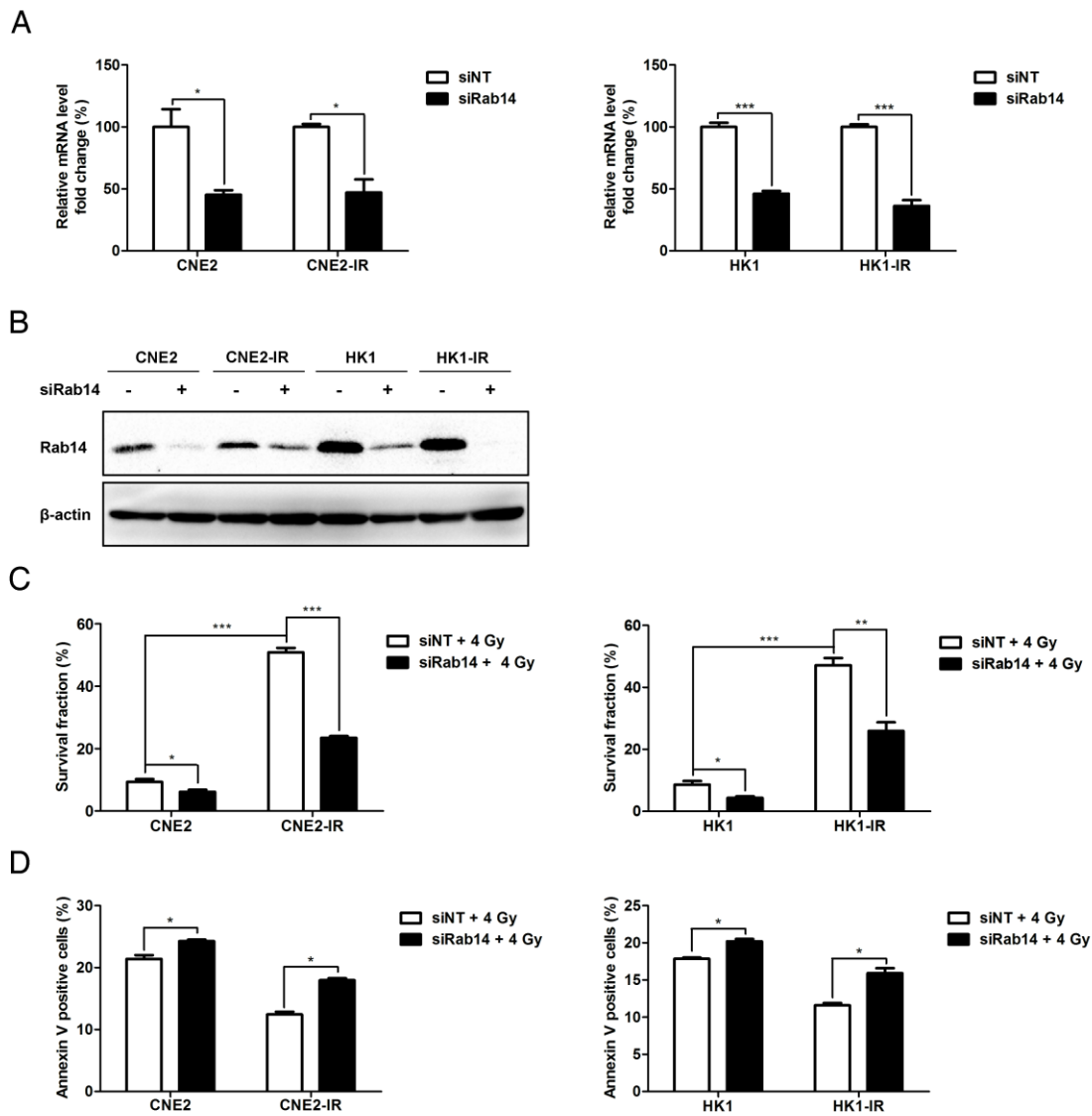


Figure S7

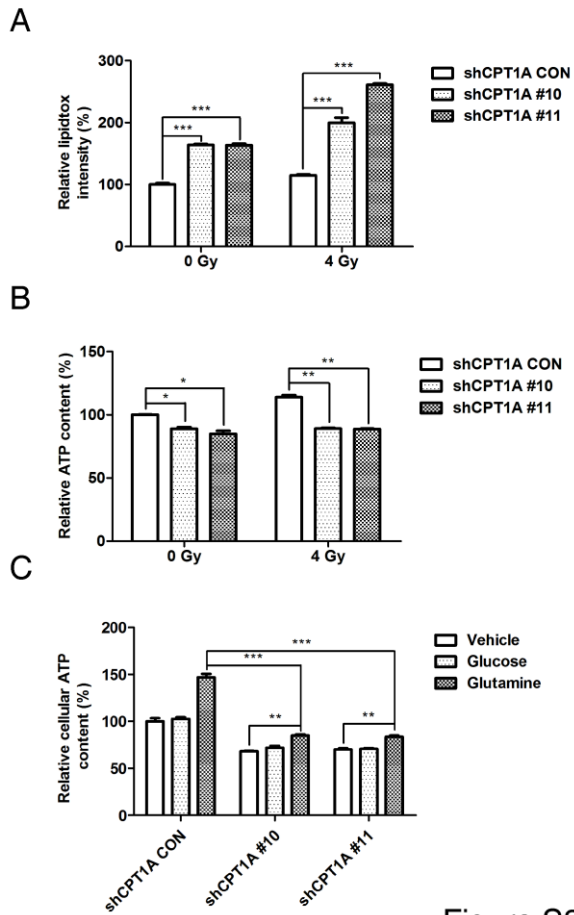


Figure S8

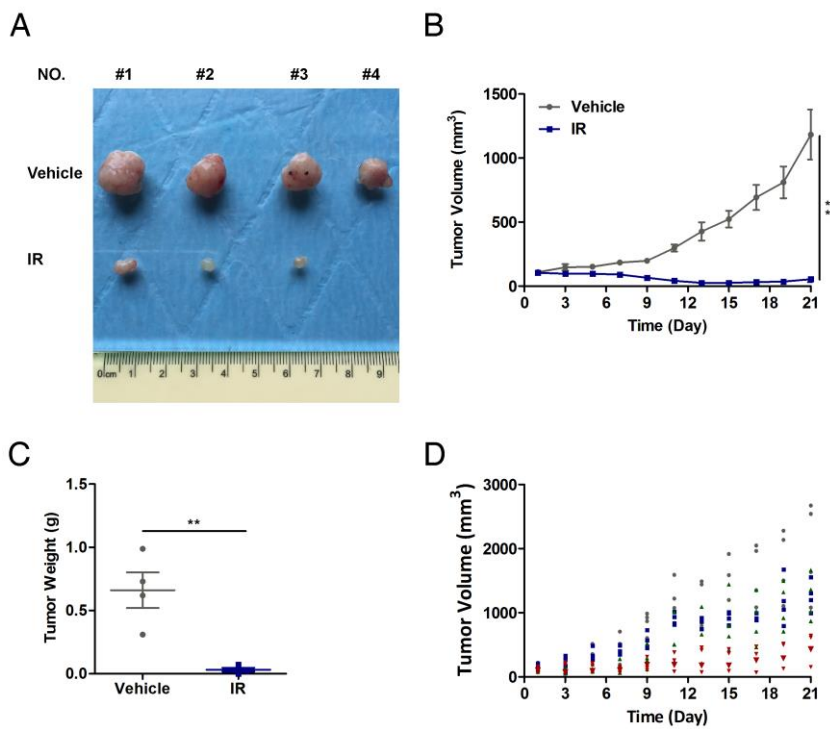


Figure S9

Supplementary Figure Legends

Figure S1. Analysis of metabolomic data and fatty acid oxidation activity (supplement to

Figure 1). (A) Fold change in cellular glycerophosphocholine and glycerophosphoethanolamine levels in CNE2-IR cells compared with CNE2 cells ($*p < 0.05$, $**p < 0.01$, $***p < 0.001$). (B) Fold change of cellular glycerophosphorylcholine and glycerol 3-phosphate levels in the groups indicated in (A). Five replicates were tested for each cell line ($***p < 0.001$). (C) Fold change of cellular palmitoyl sphingomyelin and stearoyl sphingomyelin levels in groups indicated in (A) ($***p < 0.001$). (D) Percentage of OCR relative to basal OCR of each group with the indicated treatments according to Figure 1 E ($*p < 0.05$, $**p < 0.01$, $***p < 0.001$).

Figure S2. Inhibitory effects of cisplatin and Etomoxir on NPC cells (supplement to Figure 2).

(A) Colony formation of CNE2-IR and HK1-IR cells compared with parental cells treated with a single dose of 0, 2, 4, or 6 Gy IR. (B) Colony formation assay showing survival fractions of groups indicated in (A). Survival fractions were calculated by comparing the colony number of each treatment group with untreated groups (0 Gy). Results are plotted as the mean survival fraction \pm S.E.M. The survival curves were drawn using the GraphPad Prism 5 software program ($*p < 0.05$, $***p < 0.001$). (C) MTS assay indicating cell viability and IC_{50} values of CNE2-IR and HK1-IR cells compared with parental cells treated with different concentrations of cisplatin or Etomoxir for 72 h. Data shown are normalized to the viability of the vehicle-treated cells. IC_{50} values were calculated using the GraphPad software program. Values represent mean values \pm S.D. of 3 independent experiments. (D) Colony formation of CNE2-IR and HK1-IR cells compared with parental cells treated or not treated with 4 Gy IR, Etomoxir (80 μ M), or cisplatin (0.8 μ M).

Figure S3. CPT1A expression levels, FAO activity and radiation resistance in CPT1A

knockdown and overexpressing NPC cells (supplement to Figure 2). (A) Immunoblot analysis of CPT1A protein levels in CNE2-IR cells stably transfected with *CPT1A* shRNA or control shRNA. β -Actin was used as a control to confirm equal loading of protein. (B) Labeling incorporation from $^{13}\text{C}_{16}$ -palmitate into palmitoyl-carnitine (C16), myristoyl-carnitine (C14) and lauroyl-carnitine (C12) in cells indicated in (A) at 24 h after exposure to 4 Gy IR. Data are shown as percentage of $^{13}\text{C}_{16}$ -C16, $^{13}\text{C}_{14}$ -C14, $^{13}\text{C}_{12}$ -C12 to the total pool of each corresponding acylcarnitine. Three replicates were tested for each cell line ($***p < 0.001$). (C) Oxygen consumption rate was measured in the cells indicated in (A) following palmitate (175 μM) injection at 24 h after exposure to 4 Gy IR. Three replicates were tested for each cell line ($***p < 0.001$). (D) Colony formation of indicated cells treated with 4 Gy IR. (E) Immunoblot analysis of CPT1A protein levels in CNE2 and HK1 cells stably expressing CPT1A or empty vector. β -Actin was used as a control to confirm equal loading of protein. (F) Colony formation assay showing survival fractions of HK1 cells stably expressing CPT1A or empty vector following treatment with 0 or 4 Gy IR. Results are plotted as the mean survival fraction \pm S.D. of 3 independent experiments ($**p < 0.01$, $***p < 0.001$).

Figure S4. Knockdown of CPT1A decreases radiation-resistance in CNE2-IR cells by activating mitochondrial apoptosis, which can be rescued by zVAD (supplement to Figure 4). (A)

Immunoblot analysis showing the expression levels of p-MLKL, MLKL, LC3 I/II in HT29, CNE2-IR, HK1-IR, CNE2 and HK1 cells at 48 h after exposure to 4 Gy IR or Etomoxir (80 μM).

β -Actin was used as a control to confirm equal loading of protein. (B) Immunoblot analysis showing

the expression levels of p-MLKL, MLKL, LC3 I/II in CNE2-IR cells stably transfected with *CPT1A* shRNA or control shRNA at 48 h after exposure to 4 Gy IR. β -Actin was used as a control to confirm equal loading of protein. (C) Immunoblot analysis showing the expression levels of CPT1A, cleaved PARP, cleaved caspase 9 and cleaved caspase 3 in the groups indicated in (B). β -Actin was used as a control to confirm equal loading of protein. (D) Flow cytometry analysis of apoptosis using Annexin V in CNE2-IR cells stably transfected with *CPT1A* shRNA or control shRNA and treated with 4 Gy IR or zVAD (20 μ M) for 48 h. Values represent mean values \pm S.D. of Annexin V intensity from 3 independent experiments ($*p < 0.05$, $**p < 0.01$). (E) Colony formation assay showing survival fractions of the groups indicated in (E). Survival fractions were calculated by comparing the colony number of each treatment group with untreated control cells. Results are plotted as the mean survival fraction \pm S.D. of 3 independent experiments ($**p < 0.01$, $***p < 0.001$).

Figure S5. Analysis of the CPT1A-Rab7A and CPT1A-Rab14 interactions, and the computational PPI prediction of CPT1A-Rab14 (supplement to Figure 5). (A)

Immunoprecipitation analysis showing the interaction of CPT1A and Rab7A in CNE2-IR and HK1-IR cells compared with parental cells. IgG served as the negative control. (B)

Immunoprecipitation analysis showing the interaction of CPT1A and Rab14 in cells indicated in (A) at 24 h after exposure to 0 or 4 Gy IR. IgG served as a negative control. (C) Confocal microscopy analysis of co-localization of CPT1A and Rab14 in CNE2-IR and HK1-IR cells compared with parental cells at 24 h after exposure to 4 Gy IR (red: CPT1A; green: Rab14; blue: DAPI; scale bar = 25 μ m). (D) Candidate binding sites on Rab14 using molecular docking-based screening. (E)

Identification of the N terminal of CPT1A. (F) The coupling strength between the N terminal of

CPT1A and Rab14 candidate binding sites through a co-evolution-based coupling strength analysis. **(G)** The binding of Rab14 with Rab-coupling protein (RCP) predicted by constrained docking analysis. **(H)** Co-expression analysis of CPT1A versus Rab14 in NPC patients. The mRNA levels of *CPT1A* and *Rab14* in these patients (n = 31) were obtained from Oncomine Database. The correlation coefficient was calculated using the GraphPad software program. **(I)** Immunoblot analysis showing translocation of CPT1A to mitochondria in CNE2-IR and HK1-IR cells compared with parental cells at 24 h after exposure to 4 Gy IR. β -Actin was used as a control to confirm equal loading of protein. Hsp60 served as a control to confirm equal loading of mitochondrial fractions.

Figure S6. Knock down of Rab14 interrupts fatty acid metabolism and radiation-resistance in CPT1A-overexpressing NPC cells (supplement to Figure 6). **(A)** Real-time PCR showing mRNA levels of *Rab14* in CNE2-EV, CNE2-CPT1A, HK1-EV and HK1-CPT1A cells transfected with *Rab14* siRNA pool or negative siRNA. Values represent mean values \pm S.D. of 3 independent experiments (** $p < 0.01$, *** $p < 0.001$). **(B)** Immunoblot analysis of Rab14 protein expression levels in the groups indicated in (A). β -Actin was used as a control to confirm equal loading of protein. **(C)** Oxygen consumption rate was measured in HK1-EV and HK1-CPT1A cells transfected with *Rab14* siRNA pool or negative siRNA following palmitate (175 μ M) injection at 24 h after exposure to 4 Gy IR. Three replicates were tested for each cell line (*** $p < 0.001$). **(D)** Flow cytometry analysis of apoptosis using Annexin V in CNE2-EV, CNE2-CPT1A, HK1-EV and HK1-CPT1A cells transfected with *Rab14* siRNA pool or negative siRNA at 48 h after exposure to 4 Gy IR. Values represent mean values \pm S.D. of Annexin V intensity obtained from 3 independent experiments (* $p < 0.05$, ** $p < 0.01$). **(E)** Confocal microscopy analysis of morphologies and subcellular location of free-fatty acids

in HK1-EV and HK1-CPT1A cells transfected with *Rab14* siRNA pool or negative siRNA treated with 4 Gy IR (red: Mito Tracker Red; green: Bodipy C16; blue: DAPI; scale bar = 25 μ m). **(F)** Pearson's coefficient analysis representing relative cellular co-localization of free-fatty acids overlapping with mitochondria in the groups indicated in (E). Data are expressed as mean values \pm S.D. of 12 independent cells of microscopy performed for each group (** $p < 0.01$, *** $p < 0.001$).

Figure S7. Knock down of Rab14 suppresses radiation-resistance in radiation-resistant NPC

cells (supplement to Figure 6). **(A)** Real-time PCR showing mRNA levels of *Rab14* in CNE2, CNE2-IR, HK1 and HK1-IR cells transfected with *Rab14* siRNA pool or negative siRNA. Values represent mean values \pm S.D. of 3 independent experiments (* $p < 0.05$, *** $p < 0.001$). **(B)**

Immunoblot analysis of Rab14 protein expression levels in the groups indicated in (A). β -Actin was used as a control to confirm equal loading of protein. **(C)** Colony formation assay showing survival fractions of cells indicated in (A) after exposure to 4 Gy IR. Survival fractions were calculated by comparing the colony number of each treatment group with untreated groups. Results are plotted as the mean survival fraction \pm S.D. of 3 independent experiments (* $p < 0.05$, ** $p < 0.01$, *** $p < 0.001$). **(D)** Flow cytometry analysis of apoptosis using Annexin V in cells indicated in (A) at 24 h after exposure to 4 Gy IR. Values represent mean values \pm S.D. of Annexin-V intensity from 3 independent experiments (* $p < 0.05$).

Figure S8. Knock down of CPT1A induces lipid accumulation and ATP deletion in

radiation-resistant NPC cells (supplement to Figure 7). **(A)** Flow cytometry analysis of cellular neutral lipid content using the LipidTOX Red probe in CNE2-IR cells stably transfected with *CPT1A*

shRNA or control shRNA at 24 h after exposure to 4 Gy IR. Values represent mean values \pm S.D. of LipidTOX Red intensity obtained from 3 independent experiments ($***p < 0.001$). **(B)** ATP levels of the groups indicated in (A). Values represent mean values \pm S.D. of ATP concentration obtained from 3 independent experiments ($*p < 0.05$, $**p < 0.01$). **(C)** ATP levels of groups indicated in (A), supplemented with glucose (25 mM) or glutamine (5 mM) before radiation treatment. Values represent mean values \pm S.D. of ATP concentration obtained from 3 independent experiments ($**p < 0.01$, $***p < 0.001$).

Figure S9. CNE2 xenografts are sensitive to radiation therapy (supplement to Figure 8). **(A)**

Representative images of CNE2 xenografts from IR and untreated groups. IR: 2 Gy of irradiation restricted to tumors. **(B)** Tumor growth curves of CNE2 xenografts in the groups indicated in (A).

Tumor volume analysis is presented as mean values \pm S.D. ($n = 4$, each group). Statistical significance of final tumor volumes was calculated using the two-tailed t test ($**p < 0.01$). **(C)**

Tumor weight was measured at the end of the experiment. Results are shown as mean values \pm S.D. ($n = 4$, each group; $**p < 0.01$). **(D)** Tumor volume of each CNE2-IR xenograft over the course of the experimental treatments is shown.